



# Influence of differential stress on the growth of wet enstatite and enstatite-forsterite reaction rims

Erik Rybacki<sup>1</sup> · Vanessa Helpa<sup>1</sup>

Received: 29 June 2018 / Accepted: 5 April 2019 / Published online: 29 April 2019  
© Springer-Verlag GmbH Austria, part of Springer Nature 2019

## Abstract

Reaction rim growth experiments provide insight into mass transport phenomena, which are important for metamorphic rock-forming processes and deformation mechanisms. We investigated the formation of enstatite single rims between quartz and forsterite and of enstatite-forsterite double rims between quartz and periclase using porous polycrystalline starting materials. About 3 wt% water was added, acting as a catalyst for reactions. Experiments of mainly 4 and 23 h duration were performed in a Paterson-type deformation apparatus at 1000 °C temperature, 400 MPa confining pressure and differential stresses between 0 and 46 MPa. The resulting reaction rim width varied between <1 μm and ≈ 23 μm, depending on duration and type of reaction product. At isostatic pressure conditions, our data indicate that rim growth is proportional to time, controlled by dissolution-precipitation at interfaces of interconnected fluid-filled pores. In contrast, under non-isostatic stress conditions the reaction rim thickness increases non-linearly with time, implying diffusion-controlled growth. The magnitude of differential stress has no systematic influence on the reaction rate. Microstructural observations suggest that deformation-induced reduction of interconnected porosity causes this change in rate-controlling mechanism. For a natural MgO-SiO<sub>2</sub> system, the results infer that fast interface-controlled reaction in the presence of high amounts of water is easily suppressed by concurrent deformation.

**Keywords** Water · Rim growth · Differential stress · Mineral reaction · Deformation

## Introduction

Grain boundary diffusion is an efficient mass transport pathway in fine-grained geological materials allowing fast mineral reaction during metamorphism and high creep rates of deforming rocks. With respect to mineral phase equilibria and reaction kinetics, existing experiments and thermodynamic calculations commonly rely on isostatic pressure conditions. However, the in-situ state of stress is usually non-isostatic with variable magnitude of the far field differential stress, depending on the geological setting and boundary conditions. At the grain scale, differential stresses may additionally result from stress concentrations at material heterogeneities or in response to volume changes associated with mineral reactions and phase transformations.

Theoretical approaches suggest that differential stresses affect the thermodynamic equilibrium conditions for minerals and the number of phases that are simultaneously present (e.g., Wheeler 2014; Vrijmoed and Podladchikov 2015; Hobbs and Ord 2016). These findings are supported by experimental investigations (Vaughan et al. 1984; Hirth and Tullis 1994; Delle Piane et al. 2009), but there is still ongoing debate if the mean or maximum principal stress determines equilibrium conditions (Richter et al. 2016).

Beside phase stability, differential stresses can also affect reaction rates. For example, the driving force for reaction can be modified by contributions of the elastic and plastic strain energy to the total Gibbs free energy (e.g., Karato 2008). Stress-induced plastic deformation may change the local point defect density and induce gradients of the chemical potential, presumably enhancing intracrystalline diffusion (Brodie and Rutter 1985). In addition, stress-induced line defects may lead to fast pipe diffusion along dislocation cores. If the deformation is high, grain size reduction by dynamic recrystallization or cataclasis are expected to enhance grain boundary diffusion. Furthermore, dilatant crack opening and propagation allow fluid infiltration into a dry system, which may strongly

---

Editorial handling: W. Guenther

✉ Erik Rybacki  
uddi@gfz-potsdam.de

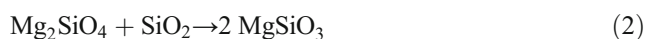
<sup>1</sup> Helmholtz Centre Potsdam German Research Centre for Geosciences – GFZ, Telegrafenberg, 14473 Potsdam, Germany

enhance reaction rates. In naturally deformed rocks enhanced metamorphic reactions via short-circuit grain boundary diffusion and grain boundary migration have been described by Keller et al. (2006, 2008) and by Terry and Heidelbach (2006), respectively. Experimental studies provide evidence for deformation-enhanced metamorphic reactions, for example in the systems feldspar-olivine (de Ronde et al. 2004; de Ronde and Stünitz 2007), periclase-ferropericlase (Heidelbach et al. 2009), calcite-dolomite (Delle Piane et al. 2009), and for  $\text{Al}_2\text{O}_3$ -polymorphs (Goergen et al. 2008). In most cases, the reaction enhancement is associated with grain size reduction and grain boundary migration at high strain deformation.

Quantitative studies on mineral reaction rates in the presence of differential stress are still rare. Few experimental studies are dealing with the formation of spinel between periclase and corundum (Keller et al. 2010; Götze et al. 2010; Jeřábek et al. 2014) and with the growth of dolomite between calcite and magnesite (Helpa et al. 2015, 2016), showing a minor influence of stress on reaction progress in most cases. In this study, we examine the geologically important system  $\text{MgO-SiO}_2$ , which was extensively investigated in isostatic reaction experiments in the past (Fisler et al. 1997; Yund 1997; Milke et al. 2001, 2007, 2009a, b; Abart et al. 2004; Gardés et al. 2011, 2012; Gardés and Heinrich 2011). At the contact between periclase ( $\text{Per} = \text{MgO}$ ) and quartz ( $\text{Qtz} = \text{SiO}_2$ ) diffusive mass transport of the components results in the formation of forsterite ( $\text{Fo} = \text{Mg}_2\text{SiO}_4$ )–enstatite ( $\text{En} = \text{MgSiO}_3$ ) double rims, following the reaction (Gardés and Heinrich 2011):



with  $\nu$  = stoichiometric coefficient ranging between 0 and 1. Enstatite single rims form between forsterite and quartz reactants, described by the reaction:



Götze et al. (2010) first investigated the influence of differential stress on enstatite-forsterite double rim growth between single crystal reactant phases. The results indicate that the double rim was thinner if grown under high differential stress of  $\Delta\sigma \approx 24$  MPa compared to rims grown at  $\Delta\sigma \approx 3$  MPa. In contrast, orthopyroxene single rims grown between polycrystalline reactants were slightly thicker if subjected to a differential stress of 29 MPa as compared to rims grown under hydrostatic conditions. However, the results are limited to few examined reaction couples and the experiments were performed in a uniaxial creep rig at atmospheric confinement and under dry conditions. Using a Paterson-type deformation apparatus, we focus here on the influence of non-isostatic stress on the formation of enstatite single rims and enstatite-forsterite double rims forming between hydrous polycrystalline reactants at high confining pressure and temperature.

## Starting materials and experimental setup

The polycrystalline reactants used in our experiments were composed of quartz sandwiched between periclase and forsterite allowing to study single and double rim evolution in a single run (Table 1, Fig. 1). Each cylindrical reactant was grinded and polished to dimensions of 7 mm diameter and 4 mm length. For some sample stacks the end surfaces of reactants were sputtered with platinum to unravel component mobility (Gardés et al. 2011). The total assembly length was 14 mm including alumina spacers on both ends. The stacks were wrapped into a thin Ni-foil and surrounded by a 0.8 mm thick talc cylinder (Fig. 2). The entire assembly was encapsulated in a steel cylinder by laser welding, which guaranteed gas-tight sealing and served as a solid buffer fixing oxygen fugacity at the Ni-NiO buffer (Mei and Kohlstedt 2000; Rybacki et al. 2006). Talc dehydrates above a temperature of  $T \approx 750$  °C at a confining pressure of  $P = 400$  MPa (Chernosky et al. 1985), releasing  $\approx 5$  wt%  $\text{H}_2\text{O}$ . This ensures wet conditions for the reaction experiments.

The average grain size of the starting materials was determined from secondary electron (SE) and back-scattered electron (BSE) micrographs using the line intercept method (Underwood 1970). Porosity was measured by He-Pycnometry (Micromeritics AccuPyc 1340), representing total connected porosity. Periclase reactants were composed of 99.7 wt%  $\text{MgO}$  with an average grain size of  $d = 13 \pm 7$   $\mu\text{m}$  and a porosity of  $\Phi = 7\%$ , fabricated by *Rauschert Heinersdorf-Pressig GmbH* (Table 1). Synthetic quartz ( $d = 130 \pm 45$   $\mu\text{m}$ ,  $\Phi = 22\%$ ) was delivered by *HiPer Ceramics GmbH*. Forsterite aggregates ( $d = 48 \pm 10$   $\mu\text{m}$ ,  $\Phi = 3\%$ ) were produced from synthetic powders by a sequence of cold isostatic pressing and subsequent hot isostatic pressing (HiP) for 23 h at  $T = 1200$  °C and  $P = 400$  MPa. The chemical composition of the forsterite was stoichiometric. In two tests (samples PO-10, PO-11, Table 3), the relatively porous and coarse-grained quartz was replaced by fine-grained natural Arkansas Novaculite (98.2 wt%  $\text{SiO}_2$ ,  $d = 4 \pm 2$   $\mu\text{m}$ ,  $\Phi = 4\%$ ) with an as-is water content of 0.21 wt% (Götze et al. 2010). Simultaneously, the coarse-grained forsterite was replaced by synthetic fine-grained forsterite ( $d = 2 \pm 1$   $\mu\text{m}$ ,  $\Phi = 7\%$ ), sintered at 1500 °C for 12 h at the *Hochschule Koblenz*. Chemical analyses showed stoichiometric composition and some isolated accumulations of impurities ( $\text{Ca} \approx 0.2$  wt%,  $\text{Al} \approx 0.08$  wt%,  $\text{Fe} \approx 0.24$  wt% and  $\text{S} \approx 0.2$  wt%).

All reaction experiments were performed at high temperature and pressure using a Paterson-type gas deformation apparatus. The target temperature, controlled by a Pt-Pt/13%Rh thermocouple, was raised with a linear heating ramp of 20 °C/min and cooled down after test termination with a rate of 2 °C/min. Reported (axial) differential stresses were determined from measured forces, corrected for the strength of talc and steel cylinders and assuming constant volume

**Table 1** Reactants grain size, porosity and water content

Phase	Abbreviation	Grain size ( $\mu\text{m}$ )	Porosity (%)	Water content* (wt%)			
				Initial reactant	Final PO-2	Final PO-3	Final PO-4
Periclase aggregate	Per_xx	$13 \pm 7$	7	0.38	0.53	0.2	0.23
Quartz aggregate	Qtz_xx	$130 \pm 45$	22	0.44	0.59	1.08	0.71
Quartz (Novaculite)	Nov_xx	$4 \pm 2$	4	0.21	–	–	–
Forsterite aggregate (HiPed)	Fo_xx	$48 \pm 10$	3	–	0.13	0.14	0.1
Forsterite aggregate (sintered)	Fo-s_xx	$2 \pm 1$	7	–	–	–	–

PO-x = sample number

\*Determined using FTIR before (initial) and after (final) experiments

deformation (Rybacki et al. 2006, 2013). Measured axial displacements were corrected for system compliance and converted to bulk axial strains with respect to the length of the entire starting material stacks. After experiments, the cylinders were cut parallel to the cylinder axis and mounted into epoxy resin. Surfaces of the mounted samples were polished with diamond paste and colloidal silica to analyse the mineral reactions at the interfaces of the starting materials.

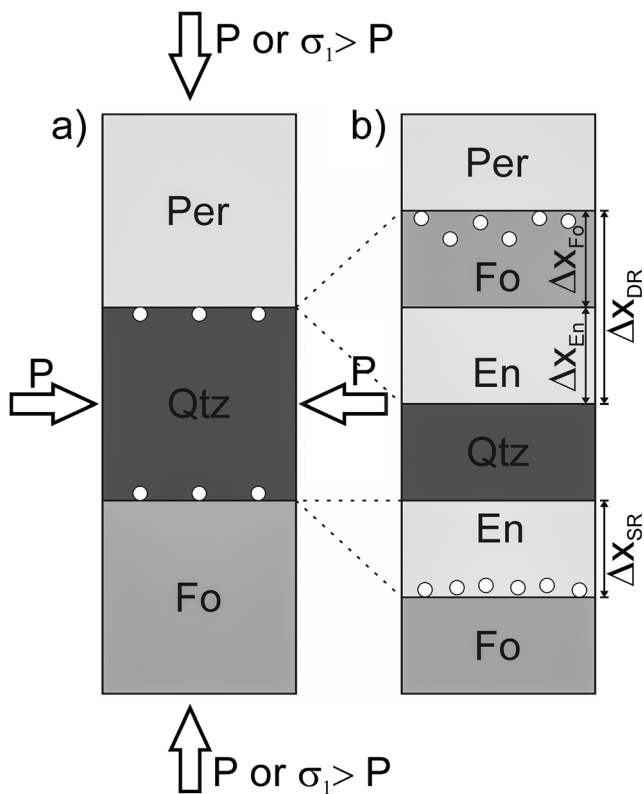


**Fig. 1** Schematic sketch of the starting assembly (a) and reaction-induced rim evolution (b). Enstatite (En) single rims are growing between quartz (Qtz) and forsterite (Fo) reactants. Enstatite – forsterite double layers form between periclase (Per) and quartz in contact. White dots indicate positions of platinum markers, see text for explanation.  $\Delta X$  = rim width,  $P$  = confining pressure,  $\Delta\sigma$  = differential stress

## Analytical methods

The average width  $\Delta x$  of each enstatite-forsterite double rim (DR) and enstatite single rim (SR) was determined from BSE images by dividing the measured total reaction rim area by the entire rim length (Table 3). In addition, the grain size of the fine-grained product phases was estimated by applying the line intercept method on BSE and SE micrographs with lines oriented parallel to the reaction interface. To amplify grain boundaries, polished surfaces were etched using 35% nitric acid for 3 to 5 min (Nishihara et al. 2016). Reported grain sizes are median values (Table 3). Detailed microstructural analyses of some samples were done using a Tecnai™G2 F20 X-twin transmission electron microscope (TEM) by applying the focused ion beam (FIB) technique (FEI FIB 200 TEM) to obtain foils with dimensions of  $17 \times 10 \times 0.15 \mu\text{m}$  cut perpendicular to the reaction interface.

The chemical compositions of the reactants and the reaction rims were analyzed using electron probe micro-analyser (EPMA, JEOL JXA-8200 Superprobe and JEOL Hyperprobe

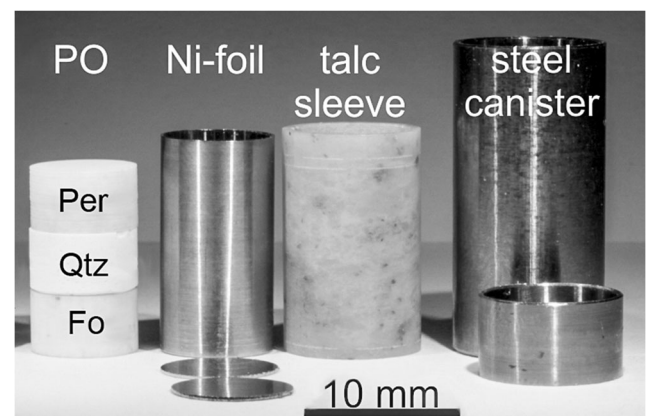


**Fig. 2** Photograph of the sample assembly. The starting materials stack (PO) fits in a hollow talc cylinder, which provides water by dehydration at experimental conditions. Both are separated by a Ni-foil, which acts as buffer and encapsulated in a steel canister

JXA-8500F). Wavelength-dispersive spectroscopy (WDS) was performed at an accelerating voltage of 10–15 kV, a beam current of 15–20 nA with a fully focused beam (~50 nm). Line scans across the reaction rims were performed using a step size of 1  $\mu\text{m}$ . Counting times were 20 s on peak and background. As calibrant materials we used olivine ( $\text{Mg}_2\text{SiO}_4$ ), diopside ( $\text{CaMgSi}_2\text{O}_6$ ) and nickel (Ni). Chemical zoning in double rims was observed by energy dispersive X-ray (EDX) element mapping using the EPMA or a scanning electron microscope (SEM Ultra 55 Plus, Carl Zeiss SMT). Maps were measured in WDS mode with dwell times of 100–400 ms and counting times of 10 s on peak and background. These settings allowed unambiguously discriminating double rims into forsterite and enstatite sublayers, utilized to determine their individual width.

The water contents of some reactant phases before and after experiments were determined using Fourier transformed infrared spectrometry (FTIR) with a Vertex 80 v interferometer and an attached IR-microscope (Hyperion 2000). The investigated samples were double polished to a thickness of 200–230  $\mu\text{m}$ . Measurements were conducted at room temperature in transmission light mode using a Globar, a KBr beam splitter and an InSb detector. Analyses were performed with an aperture size of  $130 \times 130 \mu\text{m}$  and 128 scans per spectra were averaged with a resolution of  $2 \text{ cm}^{-1}$ . After background-baseline correction and thickness normalization, the hydroxyl content was determined using the calibration given by Paterson (1982). The calculated initial intrinsic water content of synthetic periclase and quartz reactants was about 0.4 wt% (Table 1). After testing, the water contents were in the range of 0.2–1.1 wt%, roughly comparable to the starting fraction (Table 1), and of HiPed forsterite about 0.1 wt%. Unfortunately, the width of enstatite–forsterite double rims and enstatite single rims were too small to obtain reliable FTIR spectra. The total maximum water content of the sample stack was between 3.1 and 3.4 wt% (Table 2), estimated from the sum of initial water content determined by FTIR and the theoretically released amount of water by talk dehydration. At the experimental P-T conditions, water is supercritical with a density of about  $0.53 \text{ g cm}^{-3}$  (Wagner and Pruß 2002) and can be considered as a supercritical fluid with a more liquid-like character since the density is above the critical isochor (density of  $0.32 \text{ g cm}^{-3}$ ), which divides water into a material with more liquid-like and more gas-like properties.

## Results

### Bulk deformation behavior

All reaction experiments were performed at  $T = 1000 \text{ }^\circ\text{C}$  temperature and  $P = 400 \text{ MPa}$  confining pressure with run durations of 4, 8.5 or 23 h. Axial differential stresses ( $\Delta\sigma$ ) were

between 0 and 46 MPa. The resulting axial bulk strains ranged between 3% and 27% (Table 2), whereby the axial bulk strain typically increased with increasing stress. Substantial deformation of the product phases was not detected. Instead, most of the deformation was partitioned into the coarse-grained porous quartz reactant, which was shortened up to about 60% (Table 2). This demonstrates that wet porous quartz is weaker than the other minerals under the applied experimental conditions. In comparison, strong forsterite showed only minor deformation. Periclase reactants revealed slightly higher strains than forsterite, but were the weakest phase in the two sample stacks with strong Novaculite used as starting material (samples PO-10, PO-11).

Measured bulk strain-time curves showed non-linear behavior, which is typical for transient (primary) creep (Fig. 3a). Final nearly steady state creep rates of bulk sample stacks were in the order of  $\dot{\epsilon} = 10^{-7} - 10^{-6} \text{ s}^{-1}$  (Table 2), determined at about 90% - 100% of the final strain (see Fig. 3a). These creep rates are considerably higher than published steady state creep rates determined for dense wet aggregates of similar composition. For example, at our experimental P-T conditions and  $\Delta\sigma = 50 \text{ MPa}$ , which is slightly higher than the upper limit of our imposed differential stresses, existing flow laws for wet polycrystalline aggregates predict steady state strain rates for dislocation creep of quartz between  $3 \times 10^{-8} \text{ s}^{-1}$  (Paterson and Luan 1990) and  $8 \times 10^{-8} \text{ s}^{-1}$  (Rutter and Brodie 2004) and of olivine between  $2 \times 10^{-9} \text{ s}^{-1}$  (Mei and Kohlstedt 2000) and  $3 \times 10^{-9} \text{ s}^{-1}$  (Karato and Jung 2003). The low strength of our synthetic starting materials is likely caused by their high porosity, where compaction induces pronounced primary creep. Assuming a power law relation between apparent steady state creep rate and differential stress of the form

$$\dot{\epsilon} \sim \Delta\sigma^n, \quad (3)$$

where  $n$  is stress exponent, our data indicate non-linear viscous creep ( $n \approx 4$ ) at high differential stress ( $\Delta\sigma > 10 \text{ MPa}$ ) and probably Newton-viscous creep ( $n \approx 1$ ) at low differential stress (Fig. 3b).

### Reaction rim composition and microstructure

At the imposed P-T-t conditions, the mineral reaction between periclase and quartz formed double rims of enstatite and forsterite, with enstatite next to quartz and forsterite adjacent to periclase (Figs. 4a-f and 5a, c). Single enstatite reaction rims formed in between quartz and forsterite reactants, (Figs. 4g-i and 5b, d). Chemical analyses using WDS point analyses and EDX mapping reveal a homogenous composition of each sublayer in the double rims and of enstatite single rims. The average mol fractions of Mg in forsterite and enstatite rims are  $28 \pm 1 \text{ mol}\%$  and  $20 \pm 2 \text{ mol}\%$ , respectively, close to ideal



**Table 2** Reaction conditions and experimentally imposed strains

Sample	Total water content <sup>a</sup> (wt%)	Differential stress (MPa)	Time (h)	Bulk axial strain	Bulk strain rate <sup>b</sup> (s <sup>-1</sup> )	$\epsilon_{\text{Periclase}}$	$\epsilon_{\text{Quartz}}$	$\epsilon_{\text{Forsterite}}$
PO-6	3.4	0	4	0	0	0	0	0
PO-1	3.4	0	8.5	0	0	0	0	0
PO-9	3.4	0	23	0	0	0	0	0
PO-8	3.4	5	23	0.06	$1.2 \times 10^{-7}$	0.04	0.19	0.01
PO-11	3.1	6	23	0.03	$1.0 \times 10^{-7}$	0.06	0.02	0
PO-5	3.4	22	23	0.14	$2.0 \times 10^{-7}$	0.04	0.35	0.01
PO-3	3.4	32	23	0.27	$6.4 \times 10^{-7}$	0.12	0.59	0.02
PO-4	3.4	34	4	0.22	$1.2 \times 10^{-6}$	0.02	0.61	0.02
PO-2	3.4	36	4	0.09	$2.4 \times 10^{-6}$	0.02	0.26	0.02
PO-10	3.1	46	23	0.21	$1.1 \times 10^{-6}$	0.31	0.02	0.09

All experiments were performed at 1000 °C temperature and 400 MPa confining pressure

$\epsilon_{xx}$  = axial strain of component xx

<sup>a</sup> The total water content is calculated from dehydration of talc and the intrinsic water fraction

<sup>b</sup> Determined at  $\approx 90\%$  of final bulk axial strain

chemical composition. Only in two experiments using the contaminated fine-grained sintered forsterite, trace elements of Al, Ca, Fe, S and P were detected. These elements are preferentially incorporated into the enstatite (sub-) layer as indicated by a high density contrast in BSE images. Locally, high Ca substitution formed some solid solution of clinopyroxene.

Enstatite-forsterite double layers are relatively constant in thickness along the interface. Under isostatic conditions, enstatite sublayers exhibit elongated grains growing approximately perpendicular to the interface into the quartz reactant (Fig. 4a), which are less elongated at non-zero differential stress (Fig. 4b-f). The enstatite grains always contain one set of straight thin lamellae regardless of stress conditions, possibly caused by the displacive proto- to orthoenstatite transition below 1000 °C (Milke et al. 2007). The forsterite sublayers contain pores (Fig. 4), which are at least partly inherited from

the porous starting materials since they are less abundant in samples where low porous Novaculite was used as starting material (Fig. 4b, c, Table 3). This suggests that the double rim layer is preferentially growing into the quartz reactant, which is supported by the position of platinum markers that often remain near the periclase-forsterite interface (Fig. 4c). Note, however, that the alignment of particles bulge sometimes up to  $\approx 30\text{--}50\%$  of the double rim width towards the forsterite-enstatite interface, partially decorating grain boundaries and pores (e.g., Fig. 4c, left white arrow). Forsterite in contact to enstatite often shows elongated grains and sometimes an increasing grain size towards the periclase reactant (Fig. 5a, c). The latter implies that forsterite nucleation occurred at the enstatite interface and coarsened during reaction progress (cf. Gardés et al. 2012; Nishihara et al. 2016). Abundant micropores occur mainly at low differential stress within the forsterite sublayer and partially form a gap between

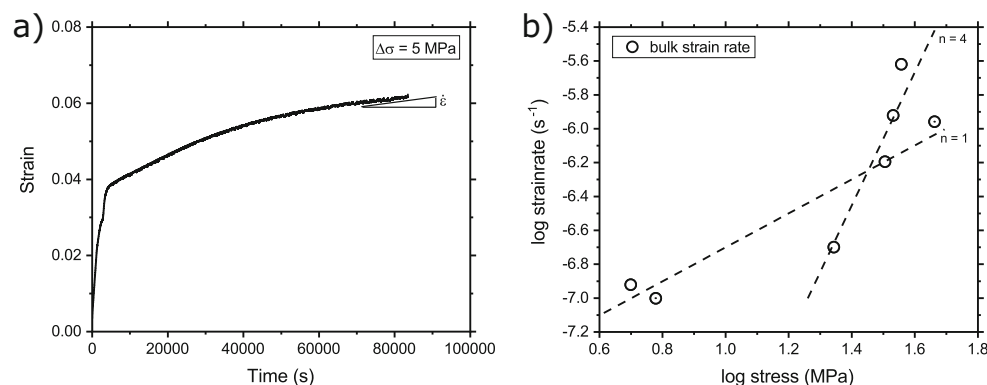
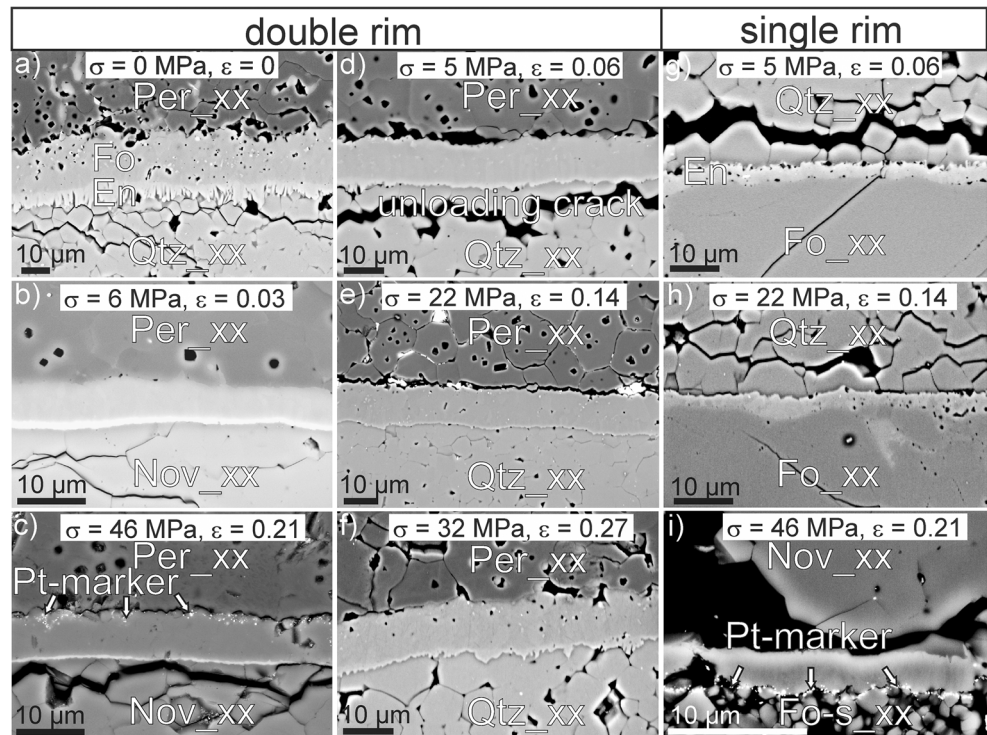


**Fig. 3** Bulk deformation behavior. **a** Typically, strain-time curves show strain hardening behavior (sample Po8, deformed at  $\Delta\sigma = 5$  MPa for  $t = 23$  h).  $\dot{\epsilon}$  is apparent steady state strain rate determined between 90 and 100% of total strain. **b** Double-logarithmic stress strain rate diagram of all

non-isostatic experiments. Symbols with central dot denote fine-grained starting material (Novaculite, sintered forsterite). A slope of  $n > 1$  indicates non-linear viscous behavior

**Fig. 4** Backscattered electron images of forsterite-enstatite double rims (a-f) and enstatite single rims (g-i). Experiments were performed at  $T = 1000\text{ °C}$  for  $t = 23\text{ h}$ . Differential stresses and bulk axial strains are labelled. **a** = sample PO-9, **b** = PO-11, **c** and **i** = PO-10, **d** and **g** = PO-8, **e** and **h** = PO-5, **f** = PO-3. Differential stresses were applied perpendicular to the interfaces. In some places abundant grains are removed due to thin section preparation. Note the location of Pt-marker



periclase and forsterite (Fig. 4a-f). A reasonable explanation is deformation of the matrix that may reduce the open pore space at high differential stress.

Enstatite single rims were produced at the contact interface between forsterite and quartz. The enstatite reaction rim and

interfaces also contain abundant micropores (Fig. 4g-i), which are probably initiated by the negative reaction volume change of  $\Delta V \approx -6.5\%$ . The latter is calculated at experimental conditions using molar volumes of  $3.21 \times 10^{-5}\text{ m}^3\text{ mol}^{-1}$  for enstatite,  $4.51 \times 10^{-5}\text{ m}^3\text{ mol}^{-1}$  for forsterite,  $1.16 \times$

**Fig. 5** Transmission electron micrographs of sample PO-2 ( $\Delta\sigma = 36\text{ MPa}$ ,  $t = 4\text{ h}$ ) (a, b) and sample PO-3 ( $\Delta\sigma = 32\text{ MPa}$ ,  $t = 23\text{ h}$ ) (c, d). Forsterite-enstatite double rims evolved between periclase and quartz reactants (a, c) and enstatite single rims formed at the contact of forsterite and quartz (b, d). Dashed lines represent phase boundaries. **b** Glass and gallium are residuals from TEM foil preparation. Differential stresses were applied perpendicular to the interfaces

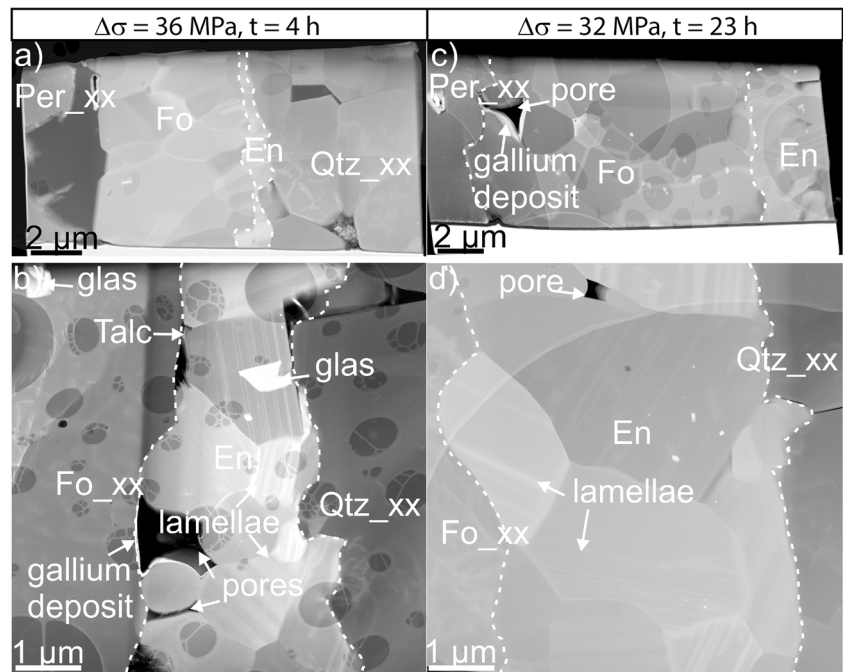


**Table 3** Reaction rim width ( $\Delta x$ ), grain size ( $d$ ) and porosity ( $\Phi$ ) of product phases

Experiment and conditions		Enstatite single rim			Enstatite/Forsterite double rim			Enstatite-DR				
Sample	Interfaces	$\Delta\sigma$ (MPa)	t (h)	$\Delta x_{En-SR}$ ( $\mu\text{m}$ )	$d_{En-SR}$ ( $\mu\text{m}$ )	$\Phi_{En-SR}$ (%)	$\Delta x_{DR}$ ( $\mu\text{m}$ )	$\Delta x_{Fo-DR}$ ( $\mu\text{m}$ )	$d_{Fo-DR}$ ( $\mu\text{m}$ )	$\Phi_{Fo-DR}$ (%)	$\Delta x_{En-DR}$ ( $\mu\text{m}$ )	$d_{En-DR}$ ( $\mu\text{m}$ )
PO-6	Per_xx/Qtz_xx	0	4	-	-	-	3.6±0.3	2.9±0.4	NA	1.3±1.1	0.7±0.2	NA
	Qtz_xx/Fo_xx			0.8±0.1	NA	1.1±0.9	-	-	-	-	-	-
PO-1	Per_xx/Qtz_xx	0	8.5	-	-	-	5.3±0.7	4.5	0.7±0.3	1.9±0.9	0.6±0.1	NA
	Qtz_xx/Fo_xx			2.0±0.4	NA	1.8±0.8	-	-	-	-	-	-
PO-9	Per_xx/Qtz_xx	0	23	-	-	-	22.7±0.7	16.8±0.7	2.0±0.9	3.6±0.9	5.9±0.1	0.9±0.5
	Qtz_xx/Fo_xx			4.4±0.6	0.7±0.3	4.0±0.7	-	-	-	-	-	-
PO-8	Per_xx/Qtz_xx	5	23	-	-	-	11.7±0.3	10.6±0.3	1.3±0.6	0.4±0.3	1.1±0.2	NA
	Qtz_xx/Fo_xx			3.7±0.2	0.7±0.3	6.8±0.2	-	-	-	-	-	-
PO-11	Per_xx/Nov_xx	6	23	-	-	-	7.5±3.2	7.4±3.5	0.9±0.4	0.1±0.1	1.2±0.9	NA
	Nov_xx/Fo-s_xx			0.8±0.2	NA	0.1±0.1	-	-	-	-	-	-
PO-5	Per_xx/Qtz_xx	22	23	-	-	-	10.9±0.6	10.5±0.6	0.9±0.3	0.7±0.2	0.6±0.2	0.5±0.2
	Qtz_xx/Fo_xx			2.6±0.2	1.2±0.4	4.0±3.8	-	-	-	-	-	-
PO-3	Per_xx/Qtz_xx	32	23	-	-	-	11.5±0.7	9.8±0.7	1.3±0.7	0.9±0.2	2.1±0.8	1.0±0.3
	Qtz_xx/Fo_xx			4.8±0.3	1.4±0.6	2.7±1.5	-	-	-	-	-	-
PO-4	Per_xx/Qtz_xx	34	4	-	-	-	4.4±0.4	3.2±0.7	0.7±0.3	1.2±1.7	1.1±0.2	NA
	Qtz_xx/Fo_xx			2.9±0.5	NA	5.1±1.8	-	-	-	-	-	-
PO-2	Per_xx/Qtz_xx	36	4	-	-	-	6.2±0.2	5.3	0.9±0.4	1.6±0.7	0.9	0.7±0.1
	Qtz_xx/Fo_xx			1.9±0.3	1.0±0.5	6.0±1.3	-	-	-	-	-	-
PO-10	Per_xx/Nov_xx	46	23	-	-	-	6.7±0.1	6.2	1.6±0.7	0.4±0.4	0.6±0.1	NA
	Nov_xx/Fo-s_xx			4.7±1.9	NA	1.0±1.8	-	-	-	-	-	-

Rim width and porosity data are arithmetic mean values. Grain sizes are median values  
*SR* single rim, *DR* double rim, *Fo* forsterite, *En* enstatite, *NA* not available

$10^{-5} \text{ m}^3 \text{ mol}^{-1}$  for periclase, and  $2.36 \times 10^{-5} \text{ m}^3 \text{ mol}^{-1}$  for quartz (calculated using the software PERPLEX by Connolly 1990, 2005 and the database of Holland and Powell 1998). The amount of pores appears to be hardly affected by the magnitude of differential stress (Fig. 4) and lower for sintered than for hipped forsterite reactants (Table 3). Platinum marker nanoparticles sputtered on interfaces in sample PO-10 aligned preferentially at the forsterite reactant interface (Fig. 4), but were occasionally also located within the enstatite layer (up to a distance of  $\approx 30\%$  of the rim width apart from the Fo-En interface). Sometimes, they appear to be associated with segregated impurities of the sintered fine-grained forsterite. Enstatite grains contain fine lamellae oriented in various directions (Fig. 5b, d). Grain boundaries of adjacent grains are usually straight or slightly curved, forming  $120^\circ$  equilibrium angles at triple junctions. This suggests minor deformation of the product phases, as also observed for double rims. Preservation of pores within reaction rims and occasionally precipitation of talc (Fig. 5b) indicate the presence of water.

### Evolution of reaction rim thickness and product grain size

The width of the reaction rims is in the range of  $\approx 4$  to  $23 \mu\text{m}$  for double rims and  $\approx 1$  to  $5 \mu\text{m}$  for single rims, respectively (Table 3). Rim growth over time is commonly expressed by a power law relationship of the form:

$$\Delta x \propto t^m \quad (4)$$

with  $\Delta x$  = rim thickness,  $t$  = time and  $m$  = rim growth exponent (e.g., Fisher 1978). Figure 6 shows the temporal evolution of reaction rim width in double-logarithmic scale. Although based on few data, our experiments indicate faster rim growth at isostatic ( $\Delta\sigma = 0$ ) than at non-isostatic conditions ( $\Delta\sigma > 0$ ). For  $\Delta\sigma = 0$  MPa (samples PO-1, 6, 9), least square fitting of the data yield a rim growth exponent of  $m_{\text{En-SR}} = 1.0 \pm 0.1$  for enstatite single rims,  $m_{\text{En-DR}} = 1.3 \pm 0.7$  for enstatite sublayer and  $m_{\text{Fo-DR}} = 1.0 \pm 0.2$  for forsterite double rims (circles in Fig. 6). These values are distinctly higher than obtained at high differential stress of  $\Delta\sigma = 33 \pm 1$  MPa (samples PO-3, 4) with corresponding values of  $m_{\text{En-SR}} = 0.3$ ,  $m_{\text{En-DR}} = 0.3$  and  $m_{\text{Fo-DR}} = 0.6$ , respectively (squares in Fig. 6).

Almost all experiments at non-isostatic conditions were terminated after 4 h or 23 h duration (Table 2). In both cases, the thicknesses of enstatite single rims and of double rim sublayers vary substantially and do not change significantly with increasing stress after 4 h run duration (Fig. 7a-c) and after 23 h duration (Fig. 7d-f). A notable exception is the relatively large double rim width at 0 MPa differential stress after  $t = 23$  h that is probably related to the very high amount of pores observed in this sample (Fig. 4a). Fast diffusion through fluid-filled pores may have accelerated rim growth

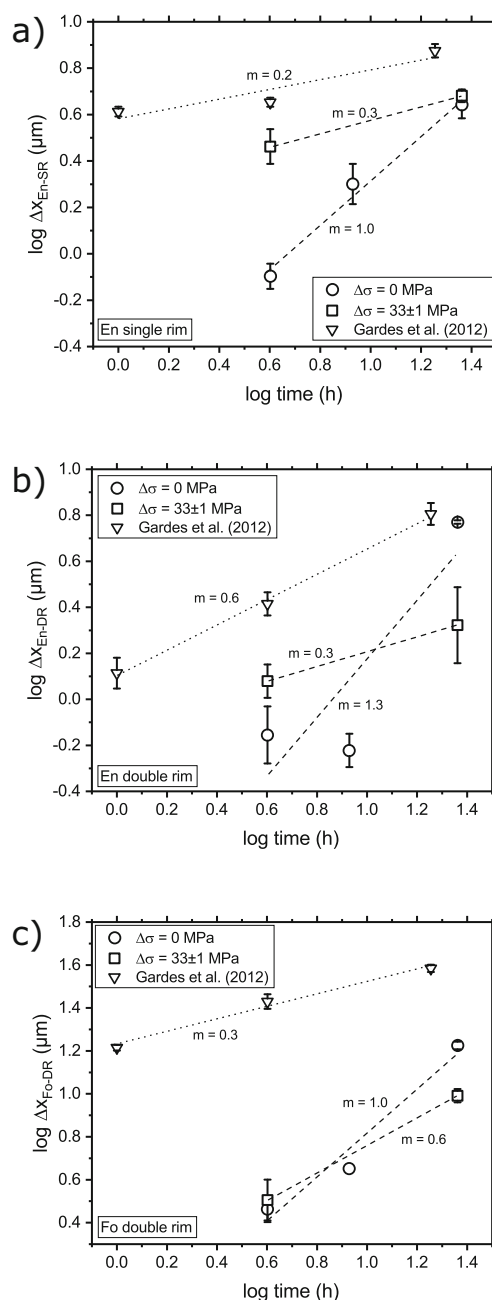
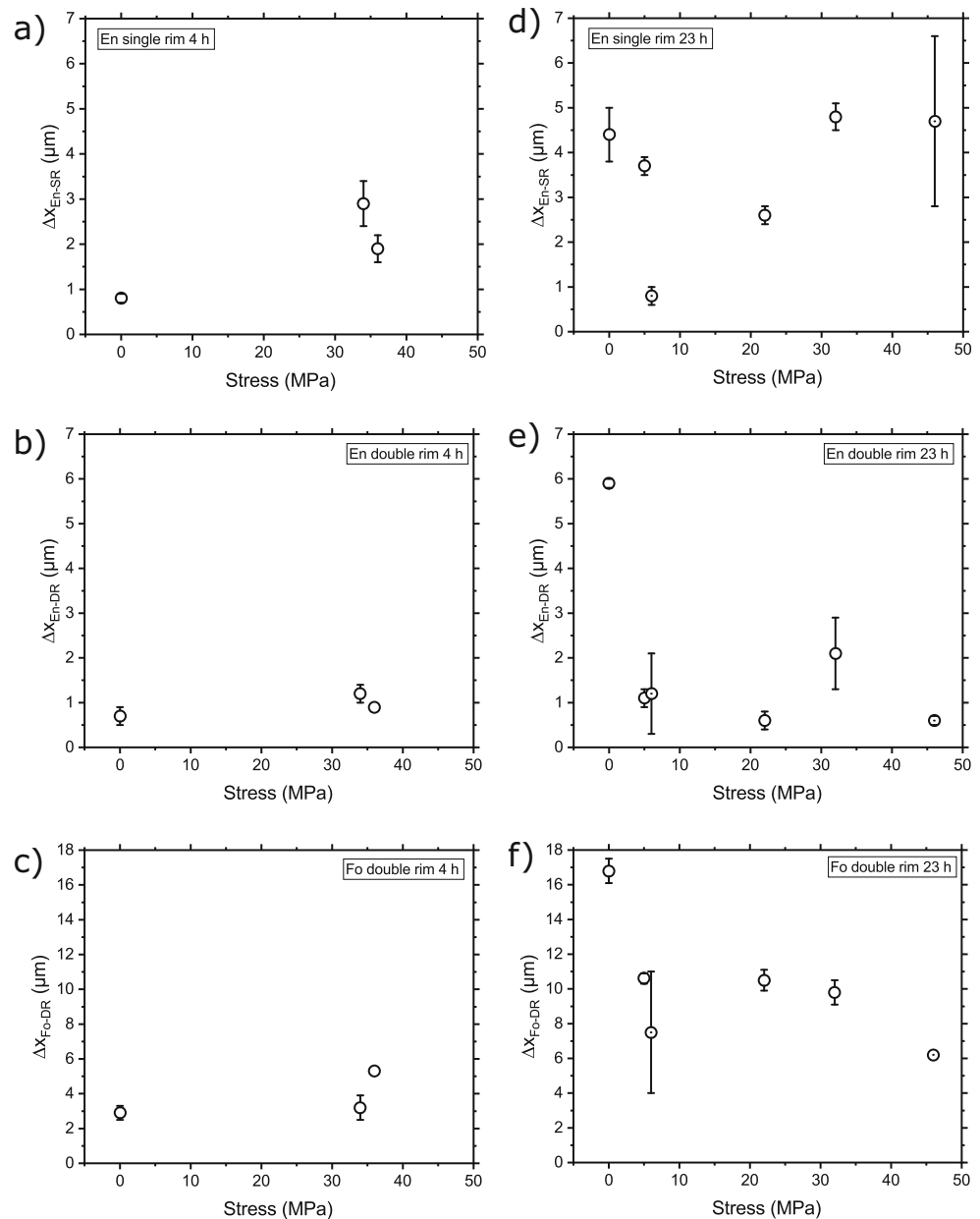


**Fig. 6** Width  $\Delta x$  of enstatite single rims (a) and of enstatite (b) - forsterite (c) sublayers in double rims versus time formed under isostatic conditions ( $\Delta\sigma = 0$  MPa, circles) and at  $\Delta\sigma = 33 \pm 1$  MPa (squares) at  $T = 1000^\circ\text{C}$ ,  $P = 400$  MPa. Isostatic ( $\Delta\sigma = 0$  MPa) data from Gardés et al. (2012) obtained on powder experiments with 1 wt% added water at  $T = 1000^\circ\text{C}$ ,  $P = 1.5$  GPa,  $P = 1.5$  GPa (triangles). The value of  $m$  represents the best fit slope. See text for discussion

in this sample compared to the remaining less porous samples, which is supported by large rim growth exponent of  $m \approx 1$  at  $\Delta\sigma = 0$  MPa (Fig. 6). The influence of the starting material porosity and grain size (synthetic quartz vs Novaculite and hipped vs sintered forsterite) appears to be minor (cf. symbols with and without central dot in Fig. 7).



**Fig. 7** Thickness  $\Delta X$  of enstatite single rims (**a, d**) and of enstatite (**b, e**) - forsterite (**c, f**) sublayers in double rims versus differential stress after  $t = 4$  h run time (**a – c**) and after  $t = 23$  h (**d – f**). The rim width is almost unaffected by  $\Delta\sigma$ . Symbols with central dot denote fine-grained starting material (Novaculite, sintered forsterite). Note different scales



Within error bars, no significant influence of differential stress on the grain size of the product phases is evident (Fig. 8). Between 4 h and 23 h duration, grain growth of the product phases is almost negligible (Table 3, Fig. 8), likely due to pinning caused by pores (Olgaard and Evans 1988). Therefore, we expect no major influence of grain size on the rim growth behavior.

## Discussion

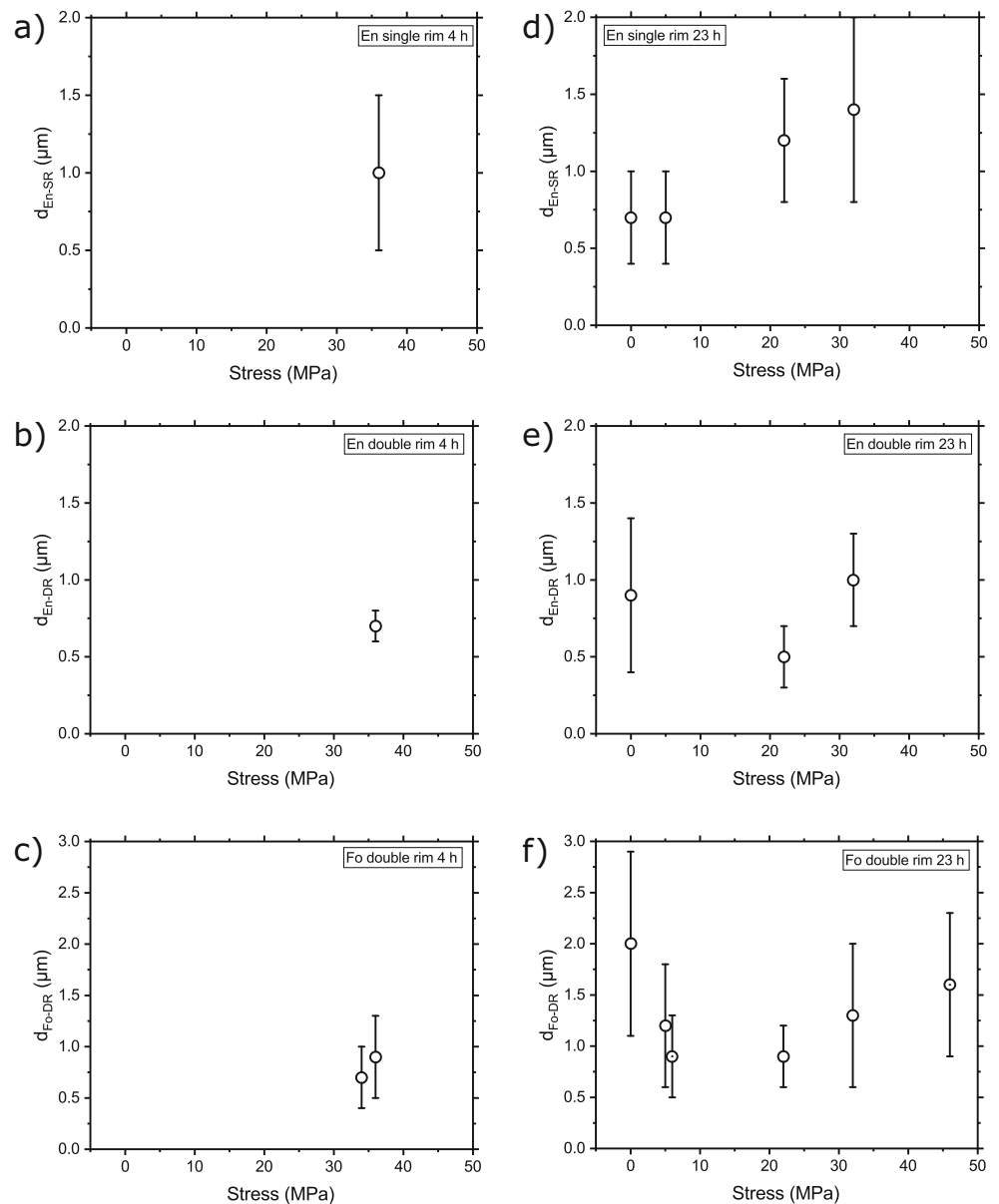
The results of our rim growth experiments on wet samples performed at  $T = 1000$  °C,  $P = 400$  MPa and  $\Delta\sigma = 0$ –46 MPa up to 23 h run duration reveal a complex rim

evolution with no systematic influence of differential stress on rim thickness and potentially higher contribution of interface-controlled reaction on rim width at isostatic than at non-isostatic conditions. We discuss plausible rim growth processes and the effect of stress on reaction kinetics.

## Effect of water on reaction rim growth

As shown in previous reaction studies in the  $\text{MgO-SiO}_2$  system performed under isostatic conditions, rim growth between fine-grained starting materials is mostly controlled by grain boundary diffusion, which is relatively insensitive to pressure, but highly sensitive to water content (e.g., Fislér et al. 1997; Yund 1997; Milke et al. 2001, 2007; Gardés et al. 2011, 2012;

**Fig. 8** Grain size  $d$  of enstatite single rims (**a, d**) and of enstatite (**b, e**) - forsterite (**c, f**) sublayers in double rims versus differential stress after  $t = 4$  h run time (**a – c**) and after  $t = 23$  h (**d – f**). Within error bars,  $\Delta\sigma$  has no effect on grain size. Symbols with central dot denote fine-grained starting material (Novaculite, sintered forsterite)



Nishihara et al. 2016). In general, the presence of only small amounts of fluids facilitates diffusion rates by enhanced solubility and enhanced diffusivity in the intergranular regions (Brady 1983; Keppler and Bolfan-Casanova 2006; Dohmen and Milke 2010). For the MgO-SiO<sub>2</sub> system, Gardés et al. (2012) specified different diffusivity regimes depending on the rock-water fraction, which are based on isostatic powder reaction experiments between crushed starting materials with grain sizes of  $\approx 1$   $\mu\text{m}$  for quartz,  $>100$   $\mu\text{m}$  for periclase and  $>200$   $\mu\text{m}$  for forsterite. At  $T = 1000$  °C and  $P = 1500$  MPa, the authors observed a transition from ‘dry’ to ‘wet’ behaviour with strongly enhanced intergranular diffusivity in a narrow water content range of 0.05–0.1 wt% H<sub>2</sub>O. Between 0.1–0.5 wt% H<sub>2</sub>O the reaction rim thickness of enstatite single rims and enstatite-forsterite double rims remained

independent of water content. Above about 0.5 wt% H<sub>2</sub>O, single and double rim width increased again, expected to reflect fast diffusion through interconnected fluid-filled pore channels (Gardés et al. 2012). As noticed by Milke et al. (2009b, 2013, 2017), the required amount of water for the transition from a dry to a wet system is substantially lower for large sandwiched samples than for fine-grained powder sample assemblies. This is because not only the total amount of water present in a system is important for enhanced grain boundary diffusion-controlled growth, but the relation between available water and grain boundary area. Because in our experiments the total water fraction was 3.1–3.4 wt% (Table 2), we expect that the reaction rims were formed in the wet, water-fraction sensitive regime, at least under isostatic conditions.

## Component mobility

Gardés et al. (2011, 2012) performed isostatic reaction rim growth experiments in the same system that we investigated. For double rim formation (Eq. (1)) the authors suggested the following partial reactions at interfaces if MgO (coupled flux of  $\text{Mg}^{2+}$  and  $\text{O}^{2-}$ ) is the only mobile component: 1) Periclase decomposes at the Per-Fo interface and mobile MgO leads to continuous formation of forsterite at the Fo-En interface:  $\text{Per} \rightarrow \text{MgO}$  with a reaction volume of  $\Delta V = -100\%$ . 2) At the Fo-En interface, the MgO flux reacts with enstatite producing forsterite according to:  $\text{MgO} + (1-f) \text{En} \rightarrow (1-f) \text{Fo} + f \text{MgO}$ , where a MgO-fraction of  $(1-f)$  is used for the reaction. The associated  $\Delta V$  is  $\approx 40\%$  for  $f=0$ . 3) At the En-Qtz interface, the remaining MgO is consumed by the partial reaction forming enstatite:  $f \text{MgO} + f \text{Qtz} \rightarrow f \text{En}$ , with  $\Delta V \approx 36\%$  for  $f=1$  (see Fig. 8 in Gardés et al. 2011). Therefore, if MgO is mobile alone, a negative reaction volume is expected only at the periclase-forsterite interface, potentially producing pores if the differential stress is low so that they cannot be closed by ongoing deformation. Our microstructural observations reveal the occurrence of pores in the whole forsterite sublayer, in particular at low differential stress, which indicates that not only MgO is mobile.

If instead  $\text{SiO}_2$  is the only mobile component in the system, the partial reactions can be formulated as: 1) Mobilization of  $\text{SiO}_2$  at the Qtz-En interface:  $2f \text{Qtz} \rightarrow 2f \text{SiO}_2$  with  $\Delta V = -100\%$  for  $f=1$ . 2) Formation of forsterite at the En-Fo interface by the partial reaction:  $2(2f-1) \text{En} + \text{SiO}_2 \rightarrow (2f-1) \text{Fo} + 2f \text{SiO}_2$  with  $\Delta V = -30\%$ . 3) Consumption of the remaining  $\text{SiO}_2$  to form forsterite at the Fo-Per interface:  $\text{SiO}_2 + 2 \text{Per} \rightarrow \text{Fo}$  with  $\Delta V = 94\%$ . In this case, pore space may be generated mainly at the quartz-enstatite interface with a high negative reaction volume, but not at the forsterite-periclase interface, where  $\Delta V$  is positive. However, the quartz-enstatite interface appears to be almost free of pores, independent of differential stress (Fig. 4), which suggests that also  $\text{SiO}_2$  is not solely mobile.

For enstatite single rim formation, the overall reaction (Eq. (2)) can be split into two half reactions (Abart et al. 2004; Milke et al. 2001). At the Fo-En interface the partial reaction is:  $\text{Fo} + k \text{SiO}_2 \rightarrow (1+k) \text{En} + (1-k) \text{MgO}$  and at the En-Qtz interface:  $(1-k) \text{MgO} + \text{Qtz} \rightarrow (1-k) \text{En} + k \text{SiO}_2$ . If we consider only MgO to be mobile ( $k=0$ ),  $\Delta V$  at the Fo-En interface is  $-29\%$  and at the En-Qtz interface  $\Delta V = 36\%$ , predicting at low stress pore formation at the Fo-En interface. If only  $\text{SiO}_2$  is mobile ( $k=1$ ), then  $\Delta V = 42\%$  at the Fo-En interface and  $\Delta V = -100\%$  at the En-Qtz interface, suggesting high porosity at low stress at the En-Qtz interface. We observed pores located on both interfaces and to some extent also in the interior of the enstatite rim (Fig. 4), which may indicate that both components are mobile.

It should be noted that the prevailing pore distribution may lead to a misinterpretation of the component mobility because part of the pores may be inherited from the preexisting porosity of the starting materials. Other diagnostic features for component mobility are related to the position of the Kirkendall plane, which marks the trace of the original contact between the reactants. This position can be marked by a discontinuous composition, microstructure or texture of reaction rims, or by initially deposited inert (Pt) markers, if they are not dragged by mobile pores, grain or phase boundaries (Gaidies et al. 2017).

We did not observe a discontinuity of the microstructure or compositions of the evolved single or double rims. Concerning the position of Pt-marker, this method is not very sensitive to identify the diffusing component, at least in the presence of water (Yund 1997). In double rim formation experiments, they should be fixed at the Per-Fo interface if only MgO is mobile, at the En-Qtz interface if only  $\text{SiO}_2$  is mobile, or at both interfaces if MgO is only mobile in forsterite and  $\text{SiO}_2$  is only mobile in enstatite (Gardés et al. 2011). We observed that the inert particles are located more close to the Per-Fo interface, but also bulge in a cloudy or wavy manner up to half of the forsterite rim width towards the Fo-En interface (Fig. 4). This finding points to both components being mobile and that the Pt-markers are sometimes dragged with moving grain boundaries or pores.

With respect to single rim formation, the Pt-marker should be located at the center of the enstatite rim if MgO diffusion predominates and at En-Qtz interface if only  $\text{SiO}_2$  is mobile. In case that both components are mobile, the marker should align at any position between the two end-members scenario (Gardés et al. 2011; Abart et al. 2004). In our experiments, however, the Pt-marker remain in most cases close to the En-Fo interface and occasionally also occur within the enstatite rim near the interface (Fig. 4). This may indicate decomposition of forsterite, so that growth occurs at the En-Qtz interface. However, in this scenario all species constituting forsterite have to be mobilized and to diffuse in the same direction towards the quartz reactant, which appears to be unlikely. Furthermore, none of the previously conducted enstatite rim growth experiments showed this behavior (e.g., Milke et al. 2001, 2009a, b; Gardés et al. 2011, 2012). Alternatively, the location of the Pt-marker may have failed to substantiate the position of the Kirkendall plane in sample PO-10, where we used this technique. In this particular experiment, we used natural Novaculite and synthetic forsterite as starting materials, which were both very fine-grained and contained 1–2 wt% impurities. We assume that pinning of the Pt-marker at impurities, wet pores and grain boundaries by surface tension forces results in continuous dragging of them at the forsterite-enstatite interface. Therefore, the deposition of inert markers does not allow to locate the position of the Kirkendall plane and to derive the mobility of components in this experiment.

Based on these considerations, we conclude that in our experiments with more than 3 wt% water both MgO and SiO<sub>2</sub> were mobile, where the latter was possibly less mobile (Abart et al. 2004, 2009). This is in accordance with rim formation tests performed by Gardés et al. (2012) under wet conditions. The authors described that SiO<sub>2</sub> was increasingly mobile, if the assemblies contained 2 wt% H<sub>2</sub>O or more, albeit distributed on a larger grain boundary area than in our experiments because we used sample stacks instead of powder sample assemblies.

### Effect of differential stress on rim growth

Even at isostatic pressure conditions the volume change associated with phase changes can locally affect the reaction rate, for example by adjusting the Gibbs energy for positive volume change or by creep of the reactants for negative volume change (Rubie and Thompson 1985; Kubo et al. 1998; Morris 2002). Schmid et al. (2009) showed that for orthopyroxene growth between dry quartz and olivine the rate of reaction progress depends on effective component diffusivity and the viscous creep response of the matrix, where the slower term will be rate limiting. Their model was derived for reaction rim growth in spherical geometry, which can be applied to powder reaction experiments. In our case we used sample stacks with initially planar interfaces, which, however, turned to rugged interfaces once the reaction is in progress (Figs. 4 and 5), so that the analysis may still be applicable. Assuming linear viscous creep, it was concluded by Schmid et al. (2009) that creep may control the progress at the early stages of reaction. In our experiments at non-isostatic conditions, the applied differential stress allows fast readjustment of the reactants by creep of the weak quartz reactant (Table 2, Fig. 3). Therefore, any retarding creep control on reaction rate is unlikely for partial reactions where enstatite formation is involved, which is always associated with a negative volume change.

From the thermodynamic point of view, the influence of differential stress on the Gibbs free energy is small compared to the contribution of pressure and temperature on the driving force for reaction (e.g., Karato 2008; Keller et al. 2010). The contributions of elastic strain energy of an incompressible solid to the total Gibbs free energy is

$$E_{el} = \frac{V_m}{2E} (\Delta\sigma)^2 \quad (5)$$

and

$$E_{pl} = \frac{1}{2} V_m \rho G b^2 \quad (6)$$

where  $E$  is Young's modulus,  $V_m$  is molar volume,  $\rho$  is dislocation density,  $G$  is shear modulus and  $b$  is the Burgers vector (Jaeger et al. 2007; Humphreys and Hatherly 2004; Keller et al. 2010). For enstatite  $E = 184,024$  MPa (Gebrande

1982),  $G = 75,700$  MPa (Gebrande 1982),  $b = 5 \times 10^{-10}$  m for slip in the system (100) [001] (Lasaga and Blum 1986; Heinisch et al. 1975) and  $\rho = 1 \times 10^{13} \text{ m}^{-2}$  (estimated from TEM images). For forsterite  $E = 195,993$  MPa (Gebrande 1982),  $G = 81,100$  MPa (Gebrande 1982),  $b = 5 \times 10^{-10}$  m (Lasaga and Blum 1986; Heinisch et al. 1975) and  $\rho = 1 \times 10^{13} \text{ m}^{-2}$  (estimated from TEM images). Inserting these values into Eqns. (5) and (6), the sum of elastic and plastic strain energy imposed by a differential stress of 50 MPa is <1% to the total driving force for enstatite single rims growth and <0.1% for forsterite formation between enstatite and periclase. Note that Eq. (5) is strictly valid only for incompressible solids with a Poisson's ratio  $\lambda$  of 0.5 or under uniaxial stress conditions. For a compressible material with  $\lambda < 0.5$  deformed in the elastic regime under triaxial conditions with principal stresses  $\sigma_1 > \sigma_2 = \sigma_3$ , the elastic strain energy density is  $E_{el} = V_m / (2E) [(\sigma_1^2 + 2\sigma_3^2) - 2\lambda(2\sigma_1\sigma_3 + \sigma_3^2)]$  (Jaeger et al. 2007). However, for our experimental conditions the increase of  $E_{el}$  compared to the incompressible case is small (<factor of 8 for  $\lambda = 0.25$ ). Therefore, the deformation-induced change of the Gibbs energy is so small that we do not expect a modification of the growth rate at non-isostatic conditions, which is in line with our observations.

Differential stress may also change the rim growth rate by microstructural modifications. For example, diffusion can be enhanced by a high point defect density or by a large amount of line defects allowing fast pipe diffusion along dislocation cores. However, the product phases appear to be relatively undeformed (Fig. 5), which suggests that the impact of a stress-induced change in defect density on diffusivity is minor in our experiments. In our experiments, increasing differential stress mainly appears to reduce the connectivity of pores, in particular at interfaces where the partial reactions predict negative reaction volumes. In addition, the dihedral angle is probably decreasing and less grain boundaries are wetted. As discussed in the following, this changes the rate-controlling mechanism under isostatic and non-isostatic conditions.

The rate controlling growth mechanism can be estimated from the time-dependence of reaction rim width. For growth controlled by interface-reaction the predicted power law exponent in Eq. (4) is  $m = 1$  (Fisher 1978). For growth controlled by volume diffusion  $m = 0.5$  (parabolic behavior). If grain boundary diffusion predominates and simultaneously grain growth occurs, the rim growth exponent  $m$  is (Gardés et al. 2011):

$$m = 0.5 \left( 1 - \frac{1}{s} \right) \quad (7)$$

where  $s$  is the grain growth exponent in the normal grain growth law (Covey-Crump 1997):

$$d^s - d_0^s \propto t, \quad (8)$$

with  $d_0$  = initial grain size.



Concerning reaction progress under dry conditions, the evolution of enstatite single rims and enstatite-forsterite double rims can be regarded as a 3-stage process, initiated first by product phase nucleation, subsequently determined by interface-reaction in the early stage of rim formation, and finally controlled by diffusion processes (Abart and Petrishcheva 2011). Under wet conditions in the regime of interconnected fluid-filled pore channels, the reaction is probably not controlled by diffusion, but by interface reaction through dissolution and precipitation processes (Gardés et al. 2012), if the reaction at the surface solid/pore fluid is slow compared to transport through the fluid (e.g., Rubie 1986; Schott et al. 2009). Although based on only few experiments, our observed rim growth exponent is  $m \approx 1$  at  $\Delta\sigma = 0$  MPa (Fig. 6), which indicates that rim growth rates are indeed controlled by interface reaction at isostatic conditions. It should be noticed, however, that the rates of dissolution and precipitation are rather complex (e.g., Lasaga 1984; Schott et al. 2009).

In contrast, at  $\Delta\sigma \approx 33$  MPa,  $m$  is about 0.3 and 0.6 for enstatite and forsterite formation, respectively (Fig. 6), but based on the results of two samples (PO-3, PO-4) with two data points at different time only. Here it is possible that we sampled a gradual transition between interface-reaction and diffusion-controlled reaction progress. Based on a thermodynamic model, Abart and Petrishcheva (2011) showed that pure parabolic growth occurs only in the case of a planar reactant geometry with perfectly mobile interfaces and that for a finite interface mobility the initial stage of rim growth is always interface-reaction controlled. Since in half of our experiments only two data points at different time for a specific rim and stress condition are available, it is possible that this gradual transition was sampled, so that the fitted exponent  $m$  do not allow to discriminate between interface-reaction and diffusion-controlled reaction progress. On the other hand, Gardés et al. (2012) did not observe such a transition in their powder reaction tests in the investigated time interval (Fig. 6). Moreover, considering additionally the other high stress samples (PO-2, PO-5 and PO-10), which seems to be justified because the magnitude of differential stress has only a minor influence on rim width (Fig. 7), results in quite similar values for enstatite single rims ( $m = 0.3 \pm 0.2$ ) and forsterite sublayers ( $m = 0.5 \pm 0.1$ ). The same procedure yields  $m = -0.2$  for enstatite double rims, but with a large uncertainty of  $\pm 0.5$  related to the low rim thickness of only  $\approx 1 \mu\text{m}$  (Table 3). Except for the last estimate, the magnitude of these  $m$  values are in the range of 0.3–0.6. For comparison, Eq. (4) predicts  $m = 0.5$  for volume diffusion and grain boundary diffusion without growth of the product grains. For any substantial grain growth Eq. (5) predicts  $m$  values  $< 0.5$ . For example, the grain growth exponent for normal grain growth in isotropic pure single-phase material is  $s = 2$ , resulting in  $m = 0.25$  and in a system containing pores or an interconnected fluid phase  $s = 3$  (Brook 1976), which gives  $m = 0.375$ . Most often,  $s$  values are

between 1 and 4 (Covey-Crump 1997), but higher values up to 20 were reported for ceramics and metals (Hidas et al. 2017; Humphreys and Hatherly 2004).

Based on this comparison of our measured rim growth exponent data determined at  $\Delta\sigma > 0$  MPa with the theoretically predicted  $m$  values, we conclude that under non-isostatic conditions grain boundary diffusion controls rim growth, probably assisted by minor grain growth.

## Comparison with other rim growth studies

### Rim growth at wet, isostatic conditions

Remarkably, at isostatic conditions Gardés et al. (2012) measured on powder samples containing 1 wt% H<sub>2</sub>O rim growth exponent values of  $m = 0.2$ – $0.6$  in the time span shown in Fig. 6. These values are quite similar to our data obtained at non-isostatic conditions. Taking also shorter runs of 8 min and 15 min duration into account, the authors obtained an average rim growth exponent of  $m \approx 0.4$  and grain growth exponents of  $s = 3.1$ – $4.2$ . Accordingly, the authors concluded that rim growth was controlled by grain boundary diffusion in conjunction with simultaneous grain growth. However, for experiments performed under isostatic conditions we estimated  $m \approx 1$ , i.e. interface reaction-controlled rim growth. We expect that the difference is caused by the dissimilar assemblies used in our and Gardés et al. (2012) experiments. Interfaces between our reactants were planar, whereas the contact areas in their powder experiments were more spherical. Accordingly, the amount of available water per unit interface area, interconnected pores and fluid films was probably higher in our assemblies than in their powder tests. These effects will enhance the proportion of interface reaction-controlled rim growth in the regime of interconnected fluid-filled pores. In line with our interpretation Gardés et al. (2012) suggested for assemblies with high water content and interconnected fluid-filled pores that the reaction rate is controlled by dissolution precipitation processes, but which could not be verified due to the lack of time series at high water fraction. Our results support their suggestion, but only under isostatic conditions.

Another notable result is the large rim width obtained by Gardés et al. (2012) for samples containing 1 wt% H<sub>2</sub>O, which are about 6 times (at 4 h) to  $\approx 2$  times (at 23 h) higher compared to our data at  $\Delta\sigma = 0$  MPa (Fig. 6). This time-dependent discrepancy can be explained by the different rate-controlling mechanisms outlined above. In addition, the reaction progress is expected to be faster for the non-planar interface geometries used in the powder experiments than for our planar reaction couples (Fisher 1978; Abart et al. 2009; Abart and Petrishcheva 2011). An alternative reason for the different rim thickness can be related to pressure, which was  $P = 1.5$  GPa in the experiments performed by Gardés et al. (2012) in a solid medium piston cylinder apparatus compared

to  $P = 0.4$  GPa in our tests applied in the gas deformation apparatus. However, the Gibbs free energy  $\Delta G_r$  for forsterite formation is about  $\approx 25$  kJ/mol at 1.5 and at 0.4 GPa pressure, determined from PERPLEX (Connolly 1990, 2005), which demonstrates that the pressure effect on rim evolution is minor. For enstatite single rim formation at  $P = 1.5$  GPa the Gibbs free energy is  $\Delta G_r = -10.1$  kJ/mol, which is almost twice than at  $P = 0.4$  GPa ( $\Delta G_r = -5.2$  kJ/mol). The higher energy potentially increases the grain boundary mobility and therefore the likelihood for nucleation of product grains above the critical size to be stable, but the measured effect of pressure appears to be small (Yund 1997).

### Rim growth at dry, non-isostatic conditions

Götze et al. (2010) performed few non-isostatic enstatite single rim and enstatite-forsterite double rim growth experiments under dry conditions using a dead load creep rig at ambient confining pressure ( $P = 0.1$  MPa). At  $T = 1250$  °C after  $t = 44.5$  h duration, they measured an increase of orthopyroxene single rim width from  $\Delta x = 9$   $\mu\text{m}$  at  $\Delta\sigma \approx 1$  MPa to  $\Delta x = 13$   $\mu\text{m}$  at  $\Delta\sigma = 24$  MPa, grown between polycrystalline quartz and olivine reactants. The increase of thickness was attributed to stress-induced compensation of the negative volume change associated with the reaction. In contrast to our tests, deformation of their dry reactants was minor. Alternatively, the authors suggested that the increase of rim width at high differential stress was caused by an increase of the grain boundary density and/or by formation of fast diffusion pathways along ‘open’ grain boundaries oriented parallel to the direction of differential stress, induced by sample extension perpendicular to the axial stress direction. The latter are expected not to occur in our experiments since we did not observe a significant change in grain size of product phases (Fig. 8) and the high confining pressure of 400 MPa in our experiments will prevent ‘opening’ of grain boundaries. Götze et al. (2010) measured also enstatite-forsterite double rim growth between single crystals reactant phases at  $T = 1350$  °C,  $P = 0.1$  MPa and  $t = 72$  h. The authors observed a reduction of the entire double rim width from  $\Delta x = 13$   $\mu\text{m}$  at  $\Delta\sigma \approx 3$  MPa to  $\Delta x = 8$   $\mu\text{m}$  at  $\Delta\sigma = 29$  MPa, associated with a reduction of the forsterite proportion from  $\approx 87\%$  to  $\approx 64\%$ . This may be caused by the positive volume change for forsterite formation and negative volume change for enstatite growth.

In our wet experiments performed at high confinement, we do not see a substantial change of double rim width with increasing differential stress except for an initial reduction at  $\Delta\sigma = 5$  MPa after 23 h duration (Table 3, Fig. 7e, f). The latter is believed to be caused by pore redistribution as explained above. Although the results of Götze et al. (2010) are based on only few experiments, we conclude that the effect of differential stress on rim growth in the MgO-SiO<sub>2</sub> system may be different for dry and wet assemblies, and largely depends on

the used configuration and P-T conditions. Further experiments are required to unravel systematic differences if they exist.

## Conclusions and geological application

Our experiments suggest that the reaction rim growth rates of enstatite single rims and enstatite-forsterite double rims are hardly influenced by the magnitude of differential stress up to about 46 MPa at the investigated P-T-t conditions. However, the reaction progress appears to change from interface-controlled growth at isostatic conditions to diffusion-controlled under non-isostatic conditions for our wet assemblies with planar interfaces. Deformation-induced reduction of the interconnectivity of fluid-filled pores associated with low wettability is likely the main reason for this switch in rate-controlling processes that occurs already at low differential stress. This suggests that rims grown under non-isostatic conditions are thinner than formed at isostatic annealing for long time scales.

Under dry conditions, however, differential stress may have an influence on the growth rate, if the reaction is coupled to a negative volume change, as indicated by the data from Götze et al. (2010). This different sensitivity to differential stress under dry and wet condition may for example explain that the formation of myrmekite during deformation of metagranites occurs preferentially at high stress sides under relatively dry conditions, but not during fluid-assisted nucleation at high strain (Menegon et al. 2006). On the other hand, other experimental data on the influence of non-isostatic stress on reaction rim growth in the systems MgO-Al<sub>2</sub>O<sub>3</sub> and CaCO<sub>3</sub>-MgCO<sub>3</sub> show that, with few exceptions, the stress effect is small compared to the impact of water, starting material microstructure, impurities, assembly geometry and loading history (Götze et al. 2010; Keller et al. 2010; Jeřábek et al. 2014; Helpa et al. 2015, 2016).

For a hypothetical scenario of shear zone development in the deep crust, stress-induced high strain deformation will lead to grain size reduction through cataclasis at low temperature or by dynamic recrystallization at high temperature. This results in enhanced reaction rates if the process is predominantly grain boundary diffusion-controlled. Inflow of water in natural shear zones will then strongly accelerate the reaction rate, as observed for example in ultramylonites (Kenkmann and Dresen 2002). The reaction progress in such a wet geological system with concurrent deformation is likely diffusion-controlled and will not turn into interface reaction-controlled regime as may be envisioned at isostatic conditions, at least for a MgO-SiO<sub>2</sub> dominated environment. The transition may be gradual since it depends on the total strain, which is stress-induced and depends on temperature, differential stress magnitude and time.

**Acknowledgements** We are grateful to Stefan Gehrmann for sample preparation, Anja Schreiber for FIB sample preparation, Michael Naumann for technical support with the Paterson apparatus, Richard Wirth for help with the TEM, Monika Koch-Müller (all Helmholtz Centre Potsdam - GFZ) for help with FTIR, Oona Appelt and Sabine Meister (Freie Universität Berlin) for help with the EPMA, and Ilona Schäpan for help with the SEM. We further like to thank Reinhard Uecker (Leibniz Institute for Crystal Growth) for providing a forsterite single crystal and Olaf Krause (University of Koblenz) for providing synthetic forsterite aggregates. The manuscript benefited from valuable discussions with Ralf Milke, Emmanuel Gardés and Petr Jeřábek. Very constructive reviews provided by Rainer Abart and an anonymous reviewer, as well as comments for handling by the Associate Editor William Guenther, improved considerably the manuscript. This work was funded by the Deutsche Forschungsgemeinschaft within the framework of FOR 741, Project RY 103/1-2, which is gratefully acknowledged.

## References

- Abart R, Petrishcheva E (2011) Thermodynamic model for reaction rim growth: Interface reaction and diffusion control. *Am J Sci* 311:517–527
- Abart R, Kunze K, Milke R, Sperb R, Heinrich W (2004) Silicon and oxygen self diffusion in enstatite polycrystals: the Milke et al. (2001) rim growth experiments revisited. *Contrib Mineral Petrol* 147:633–646
- Abart R, Petrishcheva E, Fischer FD, Svoboda J (2009) Thermodynamic model for diffusion controlled reaction rim growth in a binary system: application to the forsterite-enstatite-quartz system. *Am J Sci* 309:114–131
- Brady JB (1983) Intergranular diffusion in metamorphic rocks. *Am J Sci* 283A:181–200
- Brodie KH, Rutter EH (1985) On the relationship between deformation and metamorphism, with special reference to the behaviour of basic rocks. In: Thompson AB, Rubie DC (eds) *Metamorphic reactions. Advances in physical geochemistry*, vol 4. Springer, New York, pp 138–179
- Brook JR (1976) Controlled grain growth. In: FFY W (ed) *Ceramic fabrication processes. Treatise on materials science and technology*, vol 9. Academic Press, New York, pp 331–364
- Chernosky JV, Day HW, Caruso LJ (1985) Equilibria in the system MgO-SiO<sub>2</sub>-H<sub>2</sub>O: experimental determination of the stability of Mg-anthophyllite. *Am Mineral* 70:223–236
- Connolly JAD (1990) Multivariable phase diagrams: an algorithm based on generalized thermodynamics. *Am J Sci* 290:666–718
- Connolly JAD (2005) Computation of phase equilibria by linear programming: a tool for geodynamic modeling and its application to subduction zone decarbonation. *Earth Planet Sci Lett* 236:524–541
- Covey-Crump SJ (1997) The normal grain growth behaviour of nominally pure calcitic aggregates. *Contrib Mineral Petrol* 129:239–254
- de Ronde AA, Stünitz H (2007) Deformation-enhanced reaction in experimentally deformed plagioclase-olivine aggregates. *Contrib Mineral Petrol* 153:699–717
- de Ronde AA, Heilbronner R, Stünitz H, Tullis J (2004) Spatial correlation of deformation and mineral reaction in experimentally deformed plagioclase-olivine aggregates. *Tectonophysics* 389:93–109
- Delle Piane C, Wilson CJL, Burlini L (2009) Dilatant plasticity in high-strain experiments on calcite-muscovite aggregates. *J Struct Geol* 31:1084–1099
- Dohmen R, Milke R (2010) Diffusion in polycrystalline materials: grain boundaries, mathematical models, and experimental data. In: Zhang YX, Cherniak DJ (eds) *Diffusion in minerals and melts. Rev Mineral Geochem* 72:921–70.
- Fisher GW (1978) Rate laws in metamorphism. *Geochim Cosmochim Acta* 42:1035–1050
- Fisler DK, Mackwell SJ, Petsch S (1997) Grain boundary diffusion in enstatite. *Phys Chem Miner* 24:264–273
- Gaidies F, Milke R, Heinrich W, Abart R (2017) Metamorphic mineral reactions: Porphyroblast, corona and symplectite growth. In: Heinrich W, Abart R (eds.), *Mineral reaction kinetics: Microstructures, textures, chemical and isotopic signatures. European Mineralogical Union, Notes in Mineralogy* 16, London, pp 469–540. <https://doi.org/10.1180/EMU-notes.16.14>
- Gardés E, Heinrich W (2011) Growth of multilayered polycrystalline reaction rims in the MgO-SiO<sub>2</sub> system, Part II: modelling. *Contrib Mineral Petrol* 162:37–49
- Gardés E, Wunder B, Wirth R, Heinrich W (2011) Growth of multilayered polycrystalline reaction rims in the MgO-SiO<sub>2</sub> system, part I: experiments. *Contrib Mineral Petrol* 161:1–12
- Gardés E, Wunder B, Marquardt K, Heinrich W (2012) The effect of water on intergranular mass transport: new insights from diffusion-controlled reaction rims in the MgO-SiO<sub>2</sub> system. *Contrib Mineral Petrol* 164:1–16
- Gebrande H (1982) Elasticity and inelasticity. In: Angenheister G (ed) *Numerical data and functional relationships in science and technology. Landolt-Börnstein vol 1. Physical properties of rocks. Springer, New York*, pp 1–238
- Goergen ET, Whitney DL, Zimmerman ME, Hiraga T (2008) Deformation-induced polymorphic transformation: experimental deformation of kyanite, andalusite, and sillimanite. *Tectonophysics* 454:23–35
- Götze LC, Abart R, Rybacki E, Keller LM, Petrishcheva E, Dresen G (2010) Reaction rim growth in the system MgO-Al<sub>2</sub>O<sub>3</sub>-SiO<sub>2</sub> under uniaxial stress. *Mineral Petrol* 99:263–277
- Heidelbach F, Terry MP, Bystricky M, Holzappel C, McCammon C (2009) A simultaneous deformation and diffusion experiment: quantifying the role of deformation in enhancing metamorphic reactions. *Earth Planet Sci Lett* 278:386–394
- Heinisch HL, Sines G, Goodman JW, Kirby SH (1975) Elastic stresses and self-energies of dislocations of arbitrary orientation in anisotropic media: olivine, orthopyroxene, calcite, and quartz. *J Geophys Res* 80:1885–1896
- Helpa V, Rybacki E, Morales LFG, Dresen G (2015) Influence of stress and strain on dolomite rim growth: a comparative study. *Contrib Mineral Petrol* 170:16. <https://doi.org/10.1007/s00410-015-1172-1>
- Helpa V, Rybacki E, Morales LFG, Dresen G (2016) Influence of grain size, water, and deformation on dolomite reaction rim formation. *Am Mineral* 101:2655–2665
- Hidas K, Tommasi A, Mainprice D, Chauve T, Barou F, Montagnat M (2017) Microstructural evolution during thermal annealing of ice-I<sub>h</sub>. *J Struct Geol* 99:31–44
- Hirth G, Tullis J (1994) The brittle-plastic transition in experimentally deformed quartz aggregates. *J Geophys Res* 99:11731–11747
- Hobbs BE, Ord A (2016) Does non-hydrostatic stress influence the equilibrium of metamorphic reactions? *Earth Sci Rev* 163:190–233
- Holland TJB, Powell R (1998) An internally consistent thermodynamic dataset for phases of petrologic interest. *J Metamorph Geol* 16:309–343
- Humphreys FJ, Hatherly M (2004) *Recrystallization and related annealing phenomenon*, 2nd edn. Elsevier, London, 617 pp
- Jaeger JC, Cook NGW, Zimmerman RW (2007) *Fundamentals of rock mechanics*, 4th edn. Blackwell, Oxford, 469 pp
- Jeřábek P, Abart R, Rybacki E, Habler G (2014) Microstructure and texture evolution during growth of magnesio-aluminate spinel at corundum-periclase interfaces under uniaxial load: the effect of stress concentration on reaction progress. *Am J Sci* 314:940–965
- Karato S (2008) *Deformation of earth materials*. Cambridge University Press, New York, 463 pp



- Karato S, Jung H (2003) Effects of pressure on high-temperature dislocation creep of olivine. *Phil Mag A* 83:401–414
- Keller LM, Abart R, Wirth R, Schmid DW, Kunze K (2006) Enhanced mass transfer through short-circuit diffusion: growth of garnet reaction rims at eclogite facies conditions. *Am Mineral* 91:1024–1038
- Keller LM, Wirth R, Rhede D, Kunze K, Abart R (2008) Asymmetrically zoned reaction rims: Assessment of grain boundary diffusivities and growth rates related to natural diffusion controlled mineral reactions. *J Metamorph Geol* 26:99–120
- Keller LM, Götze LC, Rybacki E, Dresen G, Abart R (2010) Enhancement of solid-state reaction rates by non-hydrostatic stress effects on polycrystalline diffusion kinetics. *Am Mineral* 95:1399–1407
- Kenkmann T, Dresen G (2002) Dislocation microstructure and phase distribution in a lower crustal shearzone - an example from the Ivrea-Zone, Italy. *Int J Earth Sci (Geol Rundsch)* 91:445–458. <https://doi.org/10.1007/s00531-001-0236-9>
- Keppeler H, Bolfan-Casanova N (2006) Thermodynamics of water solubility and partitioning. In: Keppeler H, Smyth JR (eds) Water in nominally anhydrous minerals. *Rev Mineral Geochem* 62:193–230
- Kubo T, Ohtani E, Kato T, Shinmei T, Fujino K (1998) Effects of water on the  $\alpha$ - $\beta$  transformation kinetics in San Carlos olivine. *Science* 281:85–87
- Lasaga AC (1984) Chemical kinetics of water-rock interactions. *J Geophys Res* 89:4009–4025
- Lasaga AC, Blum AE (1986) Surface chemistry, etch pits and mineral-water reactions. *Geochim Cosmochim Acta* 50:2363–2379
- Mei S, Kohlstedt DL (2000) Influence of water on plastic deformation of olivine aggregates 2. Dislocation creep regime. *J Geophys Res* 105:21471–21481
- Menegon L, Pennacchioni G, Stünitz H (2006) Nucleation and growth of myrmekite during ductile shear deformation in metagranites. *J Metamorph Geol* 24:553–568
- Milke R, Wiedenbeck M, Heinrich W (2001) Grain boundary diffusion of Si, Mg, and O in enstatite reaction rims: a SIMS study using isotopically doped reactants. *Contrib Mineral Petrol* 142:15–26
- Milke R, Dohmen R, Becker HW, Wirth R (2007) Growth kinetics of enstatite reaction rims studied on nano-scale, Part I: methodology, microscopic observations and the role of water. *Contrib Mineral Petrol* 154:519–533
- Milke R, Abart R, Kunze K, Koch-Müller M, Schmid D, Ulmer P (2009a) Matrix rheology effects on reaction rim growth I: evidence from orthopyroxene rim growth experiments. *J Metamorph Geol* 27:71–82
- Milke R, Kolzer K, Koch-Müller M, Wunder B (2009b) Orthopyroxene rim growth between olivine and quartz at low temperatures (750–950°C) and low water concentration. *Mineral Petrol* 97:223–232
- Milke R, Neusser G, Kolzer K, Wunder B (2013) Very little water is necessary to make a dry solid silicate system wet. *Geology* 41:247–250
- Milke R, Heinrich W, Götze L, Schorr S (2017) New avenues in experimentation on diffusion-controlled mineral reactions. In: Heinrich W, Abart R (eds) Mineral reaction kinetics: Microstructures, textures, chemical and isotopic signatures. *European Mineralogical Union Notes in Mineralogy* 16, London, pp 5–36
- Morris SJS (2002) Coupling of interface kinetics and transformation-induced strain during pressure-induced solid–solid phase changes. *J Mech Phys Solids* 50:1363–1395
- Nishihara Y, Maruyama G, Nishi M (2016) Growth kinetics of forsterite reaction rims at high-pressure. *Phys Earth Planet Inter* 257:220–229
- Olgaard D, Evans B (1988) Grain growth in synthetic marbles with added mica and water. *Contrib Mineral Petrol* 100:246–260
- Paterson M (1982) The determination of hydroxyl by infrared absorption in quartz, silicate glasses and similar materials. *Bull Mineral* 105:20–29
- Paterson MS, Luan FC (1990) Quartzite rheology under geological conditions. In: Knipe RJ, Rutter EH (eds) *Deformation Mechanisms, Rheology and Tectonics*, Geological Society, London. Special Publication, pp 299–307
- Richter B, Stünitz H, Heilbronner R (2016) Stresses and pressures at the quartz-to-coesite phase transformation in shear deformation experiments. *J Geophys Res* 121(11):8015–8033
- Rubie DC (1986) The catalysis of mineral reactions by water and restrictions on the presence of aqueous fluid during metamorphism. *Min Mag* 50:399–415
- Rubie DC, Thompson AB (1985) Kinetics of metamorphic reactions at elevated temperatures and pressures: an appraisal of available experimental data. In: Thompson AB, Rubie DC (eds) *Metamorphic Reactions*. *Advances in Physical Geochemistry*, vol 4. Springer, New York, pp 27–79
- Rutter EH, Brodie KH (2004) Experimental intracrystalline plastic flow in hot-pressed synthetic quartzite prepared from Brazilian quartz crystals. *J Struct Geol* 26:259–270
- Rybacki E, Gottschalk M, Wirth R, Dresen G (2006) Influence of water fugacity and activation volume on the flow properties of fine-grained anorthite aggregates. *J Geophys Res* 111(16). <https://doi.org/10.1029/2005JB003663>
- Rybacki E, Evans B, Janssen C, Wirth R, Dresen G (2013) Influence of stress, temperature, and strain on calcite twins constrained by deformation experiments. *Tectonophysics* 601:20–36
- Schmid DW, Abart R, Podladchikov YY, Milke R (2009) Matrix rheology effects on reaction rim growth II: coupled diffusion and creep model. *J Metamorph Geol* 27:83–91
- Schott J, Pokrovsky OS, Oelkers EH (2009) The link between mineral dissolution/precipitation and solution chemistry. In: Oelkers EH, Schott J (eds) *thermodynamics and kinetics of water-rock interaction*. *Rev Min Geochem* 70:207–258
- Terry MP, Heidelbach F (2006) Deformation-enhanced metamorphic reactions and the rheology of high-pressure shear zones, Western gneiss region, Norway. *J Metamorph Geol* 24:3–18
- Underwood EE (1970) *Quantitative stereology*. Addison-Wesley-Langman, Reading, 274 pp
- Vaughan PJ, Green HW, Coe RS (1984) Anisotropic growth in the olivine-spinel transformation of  $Mg_2GeO_4$  under nonhydrostatic stress. *Tectonophysics* 108(3):299–322
- Vrijmoed JC, Podladchikov YY (2015) Thermodynamic equilibrium at heterogeneous pressure. *Contrib Mineral Petrol* 170:10. <https://doi.org/10.1007/s00410-015-1156-1>
- Wagner W, Pruß A (2002) The IAPWS formulation 1995 for the thermodynamic properties of ordinary water substance for general and scientific use. *J Phys Chem Ref Data* 31:387–535
- Wheeler J (2014) Dramatic effects of stress on metamorphic reactions. *Geology* 42:647–650
- Yund RA (1997) Rates of grain boundary diffusion through enstatite and forsterite reaction rims. *Contrib Mineral Petrol* 126:224–236

**Publisher's note** Springer Nature remains neutral with regard to jurisdictional claims in published maps and institutional affiliations.